Electronic Supporting Information for

High partial thermal conductivity of luminescence sites: a crucial factor for reducing the heat-induced lowering of the luminescence efficiency

Ni Luo,[ab] *Jing Xu*,[ab] *Xiyue Cheng*,[a] *ZhenHua Li*,[ac] *Yidong Huang*,[d] *Myung-Hwan Whangbo*,[*ae] *Shuiquan Deng*[*a] *and Maochun Hong*[a]

[a.] *State Key Laboratory of Structural Chemistry, Fujian Institute of Research on the Structure of Matter (FJIRSM) Chinese Academy of Sciences (CAS), 350002, Fuzhou, P. R. China*

[b.] *University of Chinese Academy of Sciences, 100049, Beijing, P. R. China*

[c.] *School of Physical Science and Technology & Lanzhou Center for Theoretical Physics, Lanzhou University, 730000 Lanzhou, P. R. China*

[d.] *Key Laboratory of Optoelectronic Materials Chemistry and Physics, FJIRSM, CAS, 350002, Fuzhou, P. R. China*

[e.] *North Carolina State University Raleigh, 27695-8204 North Carolina, USA*

Table of Contents

S1. Effect of the doped Eu^{2+} ion concentration

To verify the hypothesis that a high partial thermal conductivity of the luminescence site dissipates away the heat it generates and hence reduces the heat-induced lowering of the luminescence efficiency of phosphors, we had to use a high doping concentration of Eu^{2+} so as to reduce the computational burden. Namely, in the phosphors $Sr_{1-x}LiAl_3N_4$:$x$$Eu^{2+}$, $Sr_{2-x}Si_5N_8$:$x$$Eu^{2+}$ and $Sr_{1-x}SiN_2$:$x$$Eu^{2+}$, the doping level x = 0.25. To estimate the possible effect of the unrealistic dopant concentration on our conclusions, we calculated the thermal conductivity of SSN2:xEu at a smaller doping level, i.e., x = 0.125. This phosphor has the smallest unit cell among our investigated compounds. Our results for x = 0.125 and 0.25 are compared in Table S1.

Table S1 The partial thermal conductivities (W/m·K) related to the luminescence sites of SSN2:xEu and the Sr site of SSN2 using the RTA method.

Temperature	SSN2:0.25Eu	SSN2:0.125Eu	SSN2:**0.03**Eu	SSN2
300 K	0.014	0.021	**0.026**	0.723
500 K	0.008	0.013	**0.017**	0.434

Compared with the partial thermal conductivity of the Sr site in the host SSN2, the Eu doping at Sr sites causes strong reductions of the partial thermal conductivities, and in particular the calculated values of x = 0.25 does not differ significantly from that of x = 0.125 (Table S1). Assuming a linear relation between the doping concentration and the partial thermal conductivity within the doping range of $0.25 \geq x \geq 0.03$, one can estimate the partial thermal conductivity by extrapolating the values at x = 0.25 and x = 0.125 to the experimental nominal doping concentration, x = 0.03, as follows,

$$\frac{\kappa(Eu,12.5\%) - \kappa(Eu,25\%)}{25\% - 12.5\%} \approx \frac{\kappa(Eu,3\%) - \kappa(Eu,12.5\%)}{12.5\% - 3\%} \quad \text{(S1)}.$$

The results obtained at both T = 300 K and 500 K indicate that the decrease in the doping concentration does not significantly increase the thermal conductivity; The dramatic decrease in the partial thermal conductivity is caused by the doping even

though its concentration is very small. The doping concentration dependence of the partial thermal conductivity appears as a step function; once doping the partial thermal conductivity drops abruptly, after that it becomes a slowly varying function of the doping concentration. Of course, whether or not this is universally true should be verified with more test cases. Nevertheless, our analyses indicate that the model we constructed using relatively high doping concentration, $x = 0.25$, leads to reasonable results.

Table S2 The Eu…Eu distances present at several dopant concentrations for SLAN:Eu, SSN:Eu and SSN2:Eu.

$d_{Eu\text{-}Eu}$ (Å)	6.25%Eu	12.5%Eu	25%Eu
SLAN:Eu1	9.989	7.525	5.879
SLAN:Eu2	9.990	7.526	5.866
SSN:Eu1	9.405	6.879	5.747
SSN:Eu2	9.405	6.877	5.745
SSN2:Eu	7.379	5.973	5.544

In Table S2, we show the Eu…Eu distances present at several dopant concentrations. The shortest Eu…Eu distances is 5.544 Å at the doping concentration of 25% used in this work. Such a long distance indicates that the Eu…Eu interaction will be negligible, so the luminescent centers can be approximately considered as independent.

Table S3 The volume changes of the unit cells are normalized to that of single atoms at several dopant concentrations for SLAN:Eu, SSN:Eu and SSN2:Eu.

Volume(Å^3)/atom	Host	6.25%Eu	12.5%Eu	25%Eu
SLAN:Eu1	11.732	11.729	11.723	11.712
SLAN:Eu2		11.727	11.718	11.661
SSN:Eu1	12.402	12.398	12.393	12.390
SSN:Eu2		12.397	12.393	12.374
SSN2:Eu	14.135	14.116	14.101	14.091

The volume changes of the unit cells are normalized to that of single atoms. As

can be seen from Table S3, the change in the average volume per atom reduces a small amount with increasing the doping concentration, which is understandable, since the ionic radius of Sr^{2+} (1.26 Å) is slightly larger than that of Eu^{2+}(1.25 Å).

Table S4 The average of bond lengths (l_{av}) and distortion index (D) of EuN_n at several dopant concentrations for SLAN:Eu, SSN:Eu and SSN2:Eu.

		l_{av} (Å)				D			
	x	0	0.0625	0.125	0.25	0	0.0625	0.125	0.25
SLAN:xEu	$Eu1N_8$	2.805	2.798	2.798	2.796	0.0297	0.0307	0.0305	0.0303
	$Eu2N_8$	2.811	2.804	2.803	2.782	0.0330	0.0369	0.0352	0.0369
SSN:xEu	$Eu1N_6$	2.758	2.737	2.738	2.746	0.0562	0.0696	0.0702	0.0660
	$Eu2N_7$	2.834	2.826	2.826	2.827	0.0493	0.0611	0.0630	0.0591
SSN2:xEu	EuN_7	2.845	2.830	2.824	2.836	0.0756	0.0811	0.0798	0.0818

We also examined the index (W. H. Baur, Acta Cryst. 1974, B30, 1195) defined as $D = \frac{1}{n}\sum_{i=1}^{n}\frac{|l_i - l_{av}|}{l_{av}}$, where l_i denotes the distance from the center atom (Eu or Sr) to the ith coordinating atom (N), and l_{av} represents the arithmetic average of bond lengths. The n denotes the coordination number. As shown in Table S4, n is 6, 7, 8, respectively, for different Eu sites. In view of the coordination number, the average bond lengths and the distortion index, the coordination structures of the luminescent centers change marginally in our models with increasing the doping concentration.

Table S5 The calculated total and partial thermal conductivities of the SLAN:Eu, SSN:Eu and SSN2:Eu.

Phosphor	κ_{Eu}	κ_{total}	HILLE	Host	κ_{Sr}	κ_{total}
SLAN:Eu1	0.323	0.664	5% (very good)	SLAN	0.954	1.379
SLAN:Eu2	0.362	0.709				
SSN:Eu1	0.087	0.362	15% (good)	SSN	0.610	1.483
SSN:Eu2	0.077	0.366				
SSN2:Eu	0.014	0.061	57% (bad)	SSN2	0.723	1.428

In Table S5, we show the calculated total and partial thermal conductivities of the phosphors we studied. It must be pointed out that the site-μ related partial thermal conductivity may also contain the contributions of other atoms, e.g., the nearest neighboring atoms, because quite often a phonon mode involves the vibrations of various atoms in the crystal.

The results in Table S5 show that: 1) doping causes a large change of the thermal conductivity, 2) κ_{Eu} the partial thermal conductivity at site-Eu predicts correctly the order of the HILLE behaviors, κ_{total} can also do the work, however, its change is due to mainly that of κ_{Eu}, 3) Neither κ_{Sr} nor κ_{total} of the host materials can correctly predict the order of the HILLE behaviors.

S2. Computational details

S2.1. Details of the density functional theory (DFT) calculations

Structure optimization. All our DFT calculations were carried out using the Vienna Ab initio Simulation Package (VASP)[1-3] code within the projected-augmented wave (PAW) method[4] and the Perdew-Burke-Ernzerhof (PBE) parametrization of the generalized gradient approximation (GGA)[5] for exchange-correlation effects. The basis sets of the employed pseudopotentials of Sr, Li, Al, Si, N and Eu are $4s^24p^65s^2$, $1s^22s^1$, $3s^23p^1$, $3s^23p^2$, $2s^22p^3$ and $4f^75s^25p^66s^2$, respectively. The cutoff energy of the plane wave basis set was set at 520 eV, and the tetrahedron method with Blöchl corrections was used for integrations. The total electronic energy and each atomic force were converged to within 10^{-5} eV and -0.001 eV/Å, respectively. The Brillouin zone was integrated with the smallest allowed spacing between k-points of 0.3 $Å^{-1}$, and the generated grid was centred at the gamma point. The quasi-Newton algorithm as implemented in the VASP code was used in all structural optimizations. The LSDA+U method[6] (U_{eff} = 2.5 eV[7]) was used to treat the strongly correlated Eu 4f electrons.

S2.2. Details of *Phonopy* calculations

Phonon band structures and PPDOS. We used the *Phonopy* code[8] to obtain the phonon band structures of the hosts and phosphors as well as the projected phonon density of states (PPDOS) for various atoms. The force constants for all the hosts and phosphors were obtained through first-principles calculations on the basis of density functional perturbation theory (DFPT). In the calculations, the supercells were used for the hosts with finite atomic displacements of 0.01 Å, and the unit cells for the phosphors. (Hosts: SLAN: 144 atoms from 2 × 2 × 1 conventional cell; SSN: 120 atoms from 2 × 2 × 1 conventional cell; SSN2: 64 atoms from 2 × 1 × 2 conventional cell; Phosphors: SLAN:Eu: 36 atoms; SSN:Eu: 30 atoms; SSN2:Eu: 16 atoms). The reciprocal spaces of the conventional cells of all hosts and phosphors were sampled with the smallest allowed spacing 0.3 $Å^{-1}$ between k-points and the generated grid were centred at the gamma point, which are similar to those employed for the

structure optimization. The threshold for the total energy convergence was set at 10^{-8} eV. Instead of employing the Monkhorst-Pack scheme for the k-point mesh, the Γ-centered mesh was used. To obtain accurate atomic forces and reduce imaginary phonon modes for phosphors, the spin polarization was considered. To obtain the PPDOS, the Brillouin zone was integrated with a k-point mesh formed by dividing the reciprocal of the crystal lattice parameter in units of 0.025 $Å^{-1}$. The smearing method with width of 0.1 THz was employed in the calculation of PPDOS for atoms.

S2.3. Details of *Phono3py* calculations

The RTA method for lattice thermal conductivity. The *Phono3py* code[9] was used to calculate the phonon anharmonic properties and the lattice thermal conductivities. The second-order terms of the crystal potential[9] were used to calculated the atomic vibrations, and the third-order anharmonic terms to calculate the thermal conductivities. The third-order force constants for all hosts and phosphors were obtained using supercell method with finite atomic displacements of 0.03 Å in a unit cell. The reciprocal spaces of the conventional cells of all the hosts and phosphors were sampled with the smallest allowed spacing 0.3 $Å^{-1}$ between k-points and the generated grid were centred at the gamma point. To obtain more precise atomic forces, the threshold for the total energy convergence was set at 10^{-8} eV. The Brillouin zone was integrated with a k-point mesh formed by dividing the reciprocal of the crystal lattice parameter in units of 0.025 $Å^{-1}$.

Our calculations for only the thermal conductivity of SSN2:0.125Eu, which has the smallest supercell among the three materials we investigated, took more than three months on the computer cluster of our institute (2176 cores), while the time needed to calculate SSN2:0.0625Eu is estimated to exceed one year. That required for SSN2: 0.03Eu would be even more.

The direct method for the calculations of thermal conductivity. To confirm the accuracy of the lattice thermal conductivities, the *Phono3py* code was also used to obtain thermal conductivities using the direct solution of the linearized phonon transport Boltzmann equation[10] (see reference[9] for implementation details). The other

computational parameters are similar with that of the RTA method.

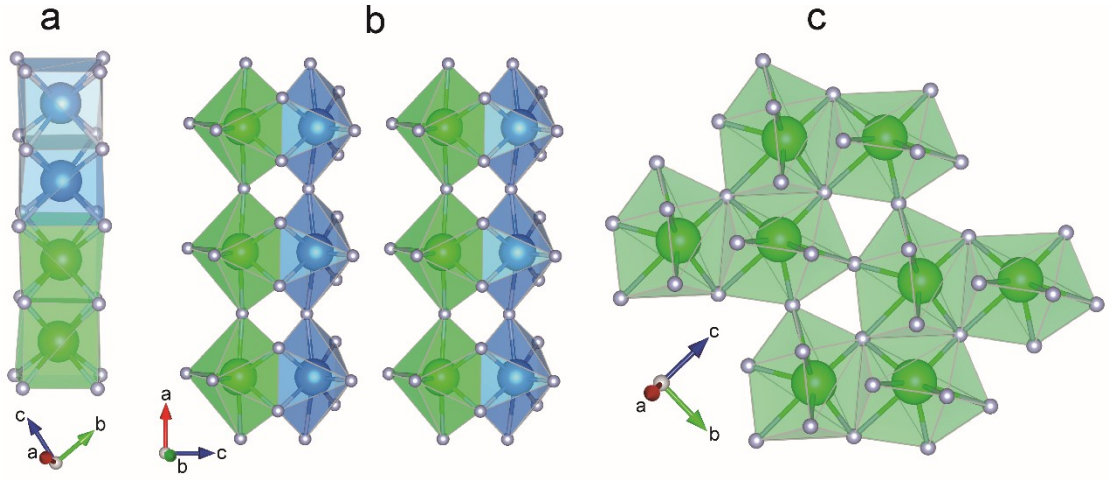

Fig. S1 The coordination environments of the Sr atoms in (a) SLAN, (b) SSN, and (c) SSN2. In SLAN, the two nonequivalent Sr atoms (Sr1 in green and Sr2 in blue spheres) form the $Sr1N_8$ and $Sr2N_8$ polyhedra, which share their opposite faces to form a chain in the [011] direction. In SSN, the Sr atoms forming the $Sr1N_6$ and $Sr2N_7$ polyhedra share their edges leading to a layer parallel to the (101) plane. In SSN2, the Sr atoms forming the SrN_7 polyhedra are condensed leading to a layer parallel to the (011) plane.

S3. Phonon bands of the three phosphors and their hosts

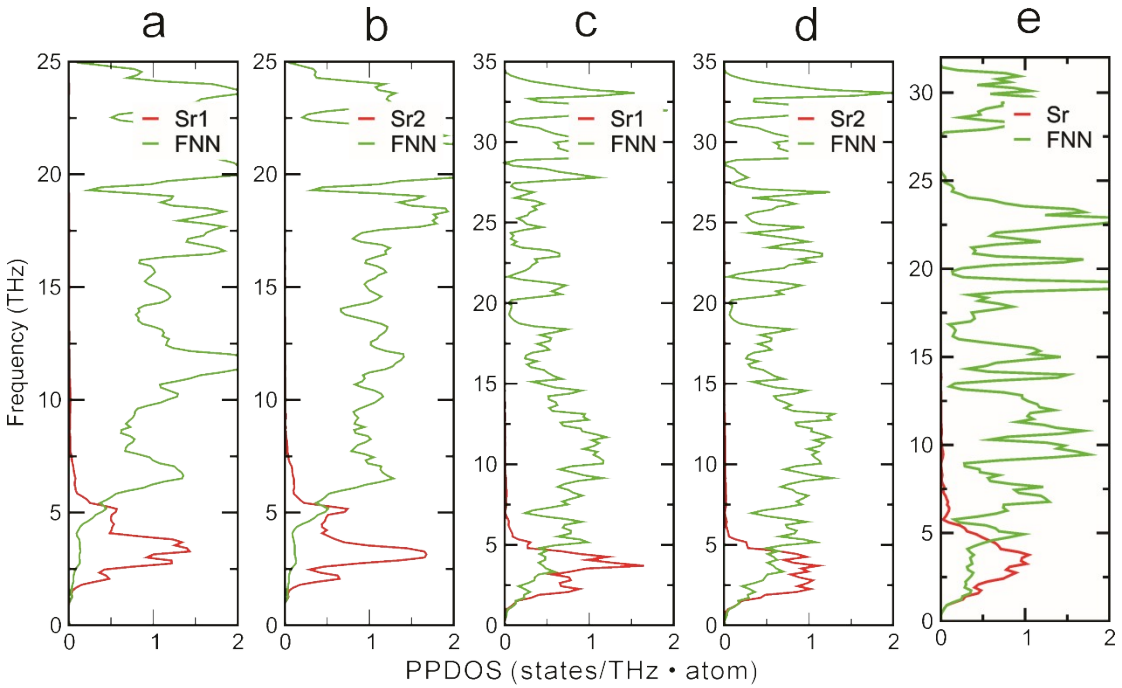

Fig. S2 PPDOS plots calculated for the Sr atoms (in red) and those of their first neighbor nitrogen atoms (in green) in (a, b) SLAN, (c, d) SSN and (e) SSN2.

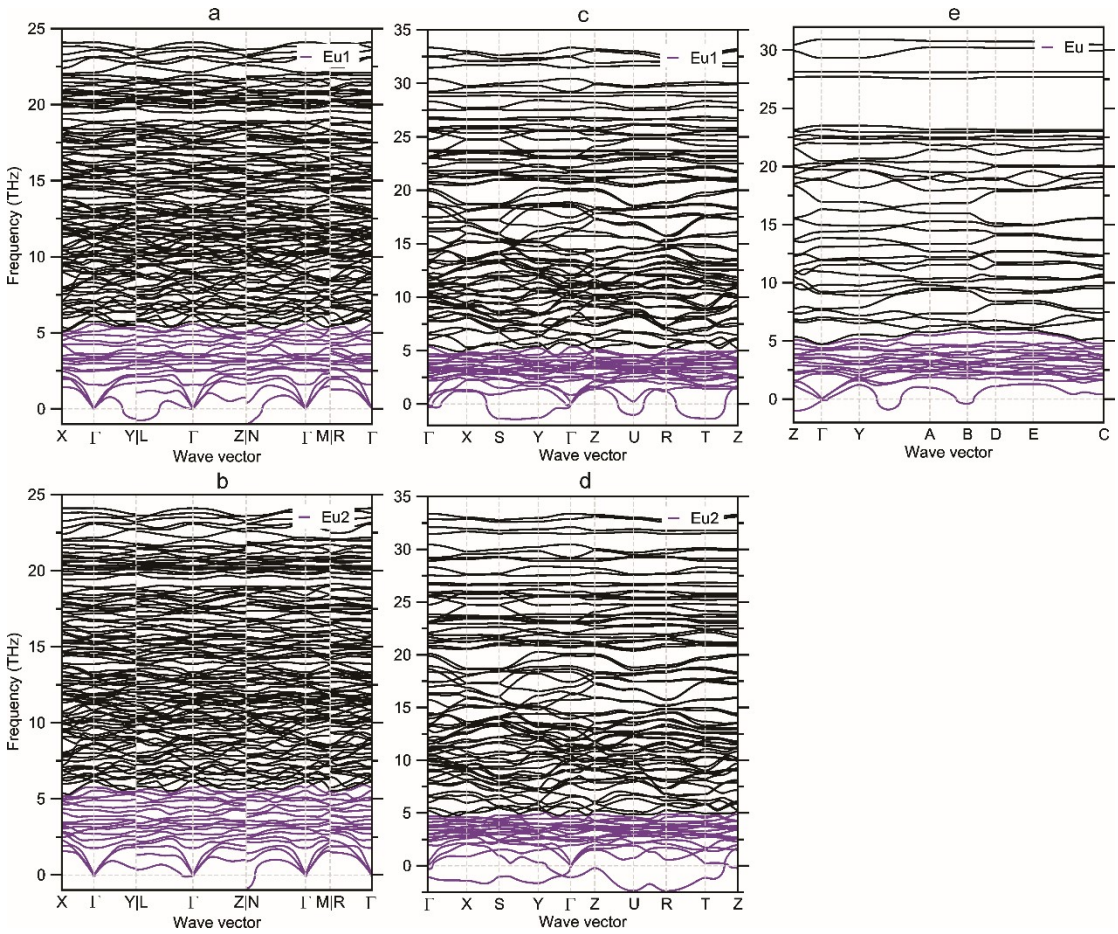

Fig. S3 Phonon band plots calculated for the phosphors (phonon modes in violet for the Eu atoms) of (a, b) SLAN:Eu, (c, d) SSN:Eu and (e) SSN2:Eu.

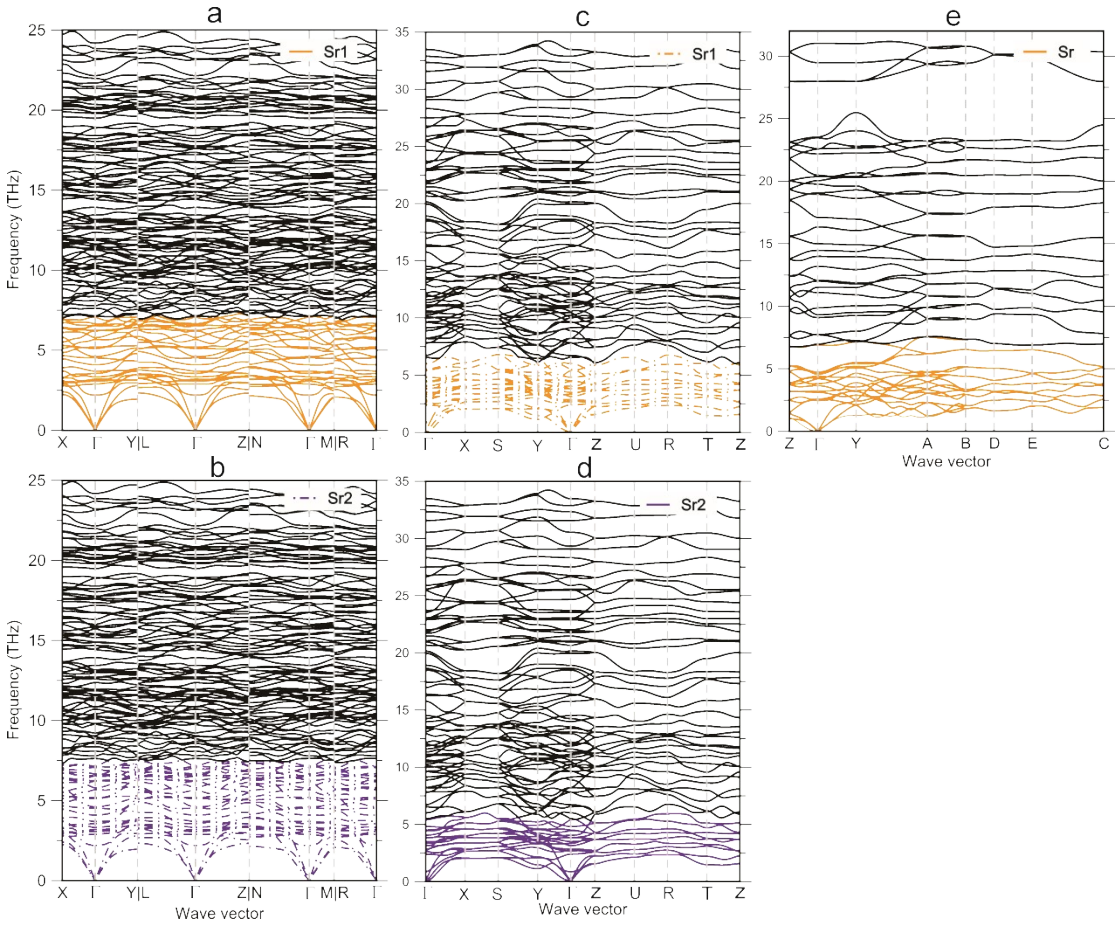

Fig. S4 Phonon band plots calculated for the hosts (phonon modes in orange for Sr(1) atoms and in indigo for Sr2 atoms) of (a, b) SLAN, (c, d) SSN and (e) SSN2.

References

1 G. Kresse and J. Hafner, *Phys. Rev. B*, 1993, **47**, 558-561.

2 G. Kresse and J. Furthmüller, *Comp. Mater. Sci.*, 1996, **6**, 15-50.

3 G. Kresse and J. Furthmüller, *Phys. Rev. B*, 1996, **54**, 11169-11186.

4 P. E. Blöchl, *Phys. Rev. B*, 1994, **50**, 17953-17979.

5 J. P. Perdew, K. Burke and M. Ernzerhof, *Phys. Rev. Lett.*, 1996, **77**, 3865-3868.

6 S. L. Dudarev, G. A. Botton, S. Y. Savrasov, C. J. Humphreys and A. P. Sutton, *Phys. Rev. B*, 1998, **57**, 1505-1509.

7 A. Chaudhry, R. Boutchko, S. Chourou, G. Zhang, N. Grønbech-Jensen and A. Canning, *Phys. Rev. B*, 2014, **89**, 155105.

8 A. Togo and I. Tanaka, *Scripta Mater.*, 2015, **108**, 1-5.

9 A. Togo, L. Chaput and I. Tanaka, *Phys. Rev. B*, 2015, **91**, 094306.

10 L. Chaput, *Phys. Rev. Lett.*, 2013, **110**, 265506.